

Detecting greatest changes in the global satellite-based precipitation observation

Majid Kazemzadeh^{1,2}, Hossein Hashemi^{2,3*}, Sadeqh Jamali⁴, Cintia B. Uvo², Ronny Berndtsson^{2,3}, and George J. Huffman⁵

¹ Faculty of Natural Resources, University of Tehran, Karaj, Iran

² Department of Water Resources Engineering, Faculty of Engineering, Lund University, Sweden

³ Centre for Advanced Middle Eastern Studies, Faculty of Social Sciences, Lund University, Sweden

⁴ Department of Technology and Society, Faculty of Engineering, Lund University, P.O. Box 118, 22 100 Lund, Sweden

⁵ NASA Goddard Space Flight Center, Code 612, 8800 Greenbelt Road, Greenbelt, MD 20771, USA

* Correspondence: hossein.hashemi@tvr.lth.se

Abstract: In recent years, analysis of abrupt and non-abrupt changes in precipitation has received much attention due to the importance of climate change-related issues (e.g., extreme climate events). In this study, we used a novel segmentation algorithm, DBEST (Detecting Breakpoints and Estimating Segments in Trend), to analyze the greatest changes in precipitation using a monthly pixel-based satellite precipitation dataset (TRMM 3B43) at three different scales (i) global, (ii) continental, and (iii) climate zone during the 1998-2019 period. We found significant breakpoints, 14.1%, both in the form of abrupt and non-abrupt changes, in the global scale precipitation at 0.05 significance level. Most of the abrupt changes were observed near the Equator in the Pacific Ocean and Asian continent relative to the rest of the globe. Most detected breakpoints occurred during 1998-1999 and 2009-2011 on the global scale. The average precipitation change for the detected breakpoint was ± 100 mm with some regions reaching ± 3000 mm. For instance, most portions of Northern Africa and Asia experienced major changes of about +100 mm. In contrast, most of the South Pacific and South Atlantic Ocean experienced changes by -100 mm during the studied period. Our findings indicated that the larger areas of Africa (23.9%), Asia (22.9%), and Australia (15.4%) experienced significant precipitation breakpoints compared to North America (11.6%), South America (9.3%), Europe (8.3%), and Oceania (9.6%). Furthermore, we found that the majority of detected significant breakpoints occurred in the arid (31.6%) and polar (24.1%) climate zones, while the least significant breakpoints were found for snow-covered (11.5%), equatorial (7.5%), and warm temperate (7.7%) climate zones. Positive breakpoints' temporal coverage in the arid (54.0%) and equatorial (51.9%) climates were more than those in other climates zones. Here, the findings indicated that large areas of Africa and Asia experienced significant changes in precipitation (-250 to +250 mm). Compared to the average state (trend during a specific period), the greatest changes in precipitation were more abrupt and unpredictable, which might impose a severe threat to the ecology, environment, and natural resources.

Keywords: Breakpoint; DBEST; Global; Precipitation; TRMM satellite

Citation: Kazemzadeh, M.; Hashemi, H.; Jamali, S.; Uvo, C.B.; Berndtsson, R.; Huffman, G.J. Detecting greatest changes in the global satellite-based precipitation observation. *Remote Sens.* **2022**, *14*, x. <https://doi.org/10.3390/xxxxx>

Academic Editor:

Received: date

Accepted: date

Published: date

Publisher's Note: MDPI stays neutral with regard to jurisdictional claims in published maps and institutional affiliations.



Copyright: © 2022 by the authors. Submitted for possible open access publication under the terms and conditions of the Creative Commons Attribution (CC BY) license (<https://creativecommons.org/licenses/by/4.0/>).

Remote Sens. **2022**, *14*, x. <https://doi.org/10.3390/xxxxx>

www.mdpi.com/journal/remotesensing

1
2
3
4
5
6
7
8
9
10
11
12
13

14
15
16
17
18
19
20
21
22
23
24
25
26
27
28
29
30
31
32
33
34
35
36
37

38
39

40
41
42
43
44
45

46 areas, especially populated regions, as well as over water bodies [3]. On regional and
47 global scales, changes in precipitation characteristics are the most relevant aspects of
48 climate change in a warming world. Yet, there is little consensus on the expected and
49 observed changes in spatiotemporal precipitation patterns [4]. While no significant
50 change in total precipitation has been detected globally [2], a notable increase in precipi-
51 tation extremes, wet and drought periods, has been observed (e.g., [5-6]) with projected
52 increases in future extremes (e.g., [7-8]).

53 The spatial pattern of precipitation changes is heterogeneous, with different regions
54 depicting opposing trends at the global scale [4, 9]. Changes in precipitation at different
55 temporal and spatial scales include not only continuous or gradual changes, which can be
56 investigated by conventional trend analysis methods (e.g., ordinary linear regression,
57 Mann-Kendall, and Mann-Whitney), but also discontinuous or abrupt changes in precipi-
58 tation amount [10]. Further, a practical problem in analyzing precipitation time series
59 is that such data are not always homogeneous and include abrupt changes in the mean
60 [11]. Abrupt changes referred to as breakpoints, or inhomogeneities, are periods of dis-
61 continuity in the time series caused by sudden changes in the climate, environment,
62 measurement techniques, observation locations, or equipment. It is noteworthy that
63 many breakpoints occur without documentation, while a breakpoint-free precipitation
64 record is less likely to occur. Therefore, before investigating the precipitation variation
65 and trends, the relative homogeneity in abrupt changes in the time series should be as-
66 sessed [12].

67 Effective identification of breakpoints in precipitation records is crucial for under-
68 standing the changes over a short period as well as detecting the causal relationships
69 between climate and environment [13]. The breakpoint detection can be conducted using
70 online (or sequential) or offline (or retrospective) approaches. A sequential approach is
71 used when it is necessary to detect the changes in real time. The retrospective breakpoint
72 detection approach is commonly used in meteorology and hydrological applications using
73 a classical statistical test to detect slope changes in the precipitation time series
74 [14-16].

75 Several techniques have been used for testing homogeneity concerning breakpoints
76 in precipitation data [11]. The Worsley's likelihood ratio test [17], cumulative deviations
77 [18], Von Neumann ratio test [18], Pettitt test [19], standard normal homogeneity test,
78 SNHT [20], and clustering approach [21] are the commonly applied techniques in the
79 precipitation breakpoint detection studies. Moreover, Vincent [22] introduced a method
80 based on the classical F and Durbin-Watson tests to detect a breakpoint in time series.
81 Seidou and Ouarda [15] proposed a Bayesian change point method to evaluate abrupt
82 changes in hydro-climatic variables.

83 Due to the large number of available statistical breakpoint detection tests, under-
84 standing the sensitivities to changes (e.g., changes in mean, median, or standard devia-
85 tion of time series) and characteristics of alternative tests is crucial to arrive at a valid in-
86 terpretation of the precipitation time series analysis. The classical statistical abrupt
87 change detection tests are sensitive to specific features such as time series mean and de-
88 viation. Thus, a statistical test that is only sensitive to a particular type of homogeneity or
89 abrupt change might not provide a comprehensive detection of abrupt changes [23-24].
90 For instance, the SNHT usually has higher sensitivity to breaks near the start and end
91 portions of the time series, while the Pettitt test is suitable to detect breaks near the mid-
92 dle part of the time series [19-20, 23]. Recently, Jamali et al. [25] developed a user-friendly
93 algorithm for the time series analysis, with two main application domains: (i) detecting
94 and characterizing trend changes and (ii) generalizing trends for main features. The
95 method in the present study, Detecting Breakpoints and Estimating Segments in Trend
96 (DBEST), uses a novel segmentation algorithm that simplifies the trend into linear seg-
97 ments with one of three user-defined parameters: the m largest changes, a generaliza-
98 tion-threshold parameter δ , or a threshold β for the magnitude of changes of interest for
99 detection. DBEST is based on Bayesian Information Criterion (BIM) [26] and statistical

tests [27] to detect statistically significant breakpoints. DBEST outputs are change type (non-abrupt or abrupt), simplified trend, and estimates for the change characteristics (magnitude and timing). DBEST is a flexible, fast, and accurate tool that is applicable to global change studies using time series of remotely sensed datasets [25].

While there are numerous studies on breakpoint detection, using standard statistical tests (e.g., Von Neumann ratio test, SNHT, and Pettitt test) in precipitation data at local and regional scales [4, 28-29], there is no comprehensive study, to the best of our knowledge, on the detection of both abrupt and non-abrupt changes at the global scale. This study focused on analyzing abrupt and non-abrupt changes at a quasi-global scale representing different climatological characteristics of precipitation of the world's wet and dry regions [4]. We applied the DBEST algorithm to detect significant breakpoints (statistically), investigate their type (non-abrupt or abrupt), and estimate their characteristics (timing and magnitude) in a quasi-global monthly satellite-based precipitation dataset over the 1998-2019 period. While evaluating abrupt and non-abrupt precipitation changes at a quasi-global scale, we investigated continental changes and their associations depending on climate zones.

2. Materials and Methods

2.1. Data sources

We used the Tropical Rainfall Measuring Mission (TRMM) Multi-satellite Precipitation Analysis (TMPA) product, in which the National Aeronautics and Space Administration (NASA) estimates quasi-global precipitation. TRMM TMPA data are produced based on the constellation of passive microwave and infrared sensors onboard multiple partners' satellites [30-31]. The core observatory, TRMM, was a collaboration between the Japan Aerospace Exploration Agency (JAXA) and NASA; it was launched in November 1997 and ended its mission in April 2015. However, the TMPA algorithm continued producing precipitation data using the partner satellites through the end of 2019. TMPA Version 7 provides products at 3-hourly (3B42), daily (3B42-derived), and monthly (3B43) temporal resolutions, in the latitude band 50°N-S at 0.25°×0.25° spatial resolution [30, 32] for the period of 1998-2019. Monthly TMPA-3B43 v7.0 is one of the most widely used products for climate and research purposes [30, 33]. It is noteworthy that the transition from TMPA to Integrated Multi-satellite Retrievals for Global Precipitation Measurement (GPM) mission (IMERG) began in 2015, and the IMERG data are now available for the 2000-present period. While IMERG provides a more detailed precipitation dataset (temporally and spatially), a thorough validation of its products continues to be conducted for use in global-scale analyses. A detailed description of the TMPA and IMERG algorithms and input data can be found in Huffman et al. [34], as well as Huffman et al. [30], Huffman and Bolvin [35], and Huffman [36].

The TRMM products have been used extensively in many regions around the world. Their spatiotemporal performance has been thoroughly validated by ground-based measurements all over the globe [37], such as in the United States [38-42], India [43-45], China [46-47], Iran [48-50], the Philippines [51], Eastern Africa [52], and Malaysia [53], to mention a few. In this study, we used the TMPA 3B43 research product at a monthly time scale from January 1998 to December 2019. The TMPA 3B43 product used in this study incorporates bias-corrected surface precipitation gauge analyses. Thus, it takes advantage of gauge information, where available, and the multi-satellite scheme everywhere.

2.2. Methods

2.2.1. Breakpoint detection

The DBEST algorithm has two main application domains: trend generalization and change detection. We used the change detection method, which is a novel segmentation algorithm that simplifies the trend into linear segments using the m largest changes or a threshold β for detection's magnitude of change of interest (Table 1).

Here, we briefly describe the DBEST's change detection workflow along with the threshold values used in this study. DBEST starts with testing the existence of significant discontinuities (or level-shift) in the precipitation input time-series. To do so, the absolute difference in precipitation between each pair of consecutive data points is compared with a user-defined *first level-shift-threshold* ($\theta_1=10$ mm in this study). If the absolute difference is greater than the threshold value θ_1 , a second criterion test whether the change led to a considerable shift in the precipitation mean level and persisted throughout the user-defined period, the *duration-threshold* ($\phi=1$ year). If the absolute difference in the mean of the precipitation data, computed over a period ϕ before and after the current data point, is greater than a user-defined *second level-shift-threshold* ($\theta_2=40$ mm), the second criterion is valid. The current data point is defined as a candidate level-shift point if both tests are valid. This repeats for every data point in the precipitation time series until all candidate points are identified. The identified points are then sorted into descending order according to the absolute value of the shift in the precipitation mean. The first point in the sorted list is listed as the most critical level-shift point. In addition to the two criteria mentioned, a third criterion should be fulfilled for the second and subsequent candidate points to be detected as the next critical level-shift point. The third criterion test is performed if the spacing between the candidate point and each previously detected level-shift point is at least the *duration-threshold* ϕ .

After examining the existence of the level-shift points, DBEST proceeds with detecting major breakpoints. To do so, for the precipitation input time series (P) with several observations N ($N>2$), single time-step differences in the forward and backward directions are computed at every time-point i ($2 \leq i \leq N-1$) as:

$$P_{(i-1,i)} = P_{(i)} - P_{(i-1)} \quad (1)$$

$$\Delta P_{(i,i+1)} = P_{(i+1)} - P_{(i)} \quad (2)$$

For each point i , the peak/valley detector function (f) is then calculated based on the continuity of the sign of two differences:

$$f(i) = \begin{cases} 1, & \text{if sign}(\Delta P_{(i-1,i)}) = -\text{sign}(\Delta P_{(i,i+1)}) \\ 0, & \text{otherwise} \end{cases} \quad (3)$$

Table 1. User-defined thresholds in the DBEST's change detection algorithm [25].

Threshold	Description
First level-shift-threshold (θ_1)	The lowest absolute difference in input data (Precipitation) between the level-shift point and next data point
Duration-threshold (ϕ)	The lowest period (time steps) within which the shift in the mean of the data level, before and after the level-shift point, persists; and the lowest spacing (time steps) between successive level-shift points.
Second level-shift-threshold (θ_2)	The lowest absolute difference in the means of the data calculated over the period ϕ before and after the level-shift point
Change number (m)	Number of greatest breakpoints of interest for detection
Statistical significance level (α)	The statistical significance level used for testing the significance of detected changes

The trend direction changes for time points at which the valley/peak detector function equals one. These are called *valley and peak* points. For all data points, a second turning

153
154
155
156
157
158
159
160
161
162
163
164
165
166
167
168
169
170
171
172
173
174
175
176
177
178
179
180
181
182
183

Field Code Changed

202
203
204

point detector function (g) is calculated based on the valley/peak detector function and an iterative criterion (refer to Jamali et al. [25]). Using this function, all potential turning points are identified (Fig. 1). The identified level-shift points are added to the turning points set. For valid turning points, a subset of turning points that significantly reduces the residual sum of squares of a least-square fits the precipitation time series and does not result in overfitting, are then determined using an iterative piecewise fitting method based on Bayesian Information Criterion (BIC) [26]. The significance of the valid turning points is tested using statistical tests ($\alpha=0.05$) for the corresponding segments in the obtained optimal model fit to the precipitation trend that minimizes the BIC [25]. The significant turning points are called *breakpoints* (Fig. 1). Note that a breakpoint can be *abrupt* or *non-abrupt* depending on whether it is a level-shift point or not, respectively. Finally, the magnitude and timing characteristics for the detected breakpoints are computed and reported as output for several greatest breakpoints of interest for detection set by the user ($m=1$). For any detected change, the corresponding breakpoint (break date) is the *start time*, and the next turning point is the *end time*. The *change duration* is the time between the start time and the end time. The *change magnitude* is calculated by subtracting the fitted precipitation value at the start time from the fitted value at the end time (Fig. 1). The sign of the obtained change value represents the *change direction* (whether the slope is decreasing or increasing); for more details, see Jamali et al. [25].

We used the DBEST algorithm for detecting and characterizing the greatest breakpoints in the TRMM TMPA 3B43 version 7 precipitation product, called "TRMM and Other Data Precipitation Data Set" at a monthly time scale during the 1998-2019 period.

205
206
207
208
209
210
211
212
213
214
215
216
217
218
219
220
221
222
223
224
225
226
227

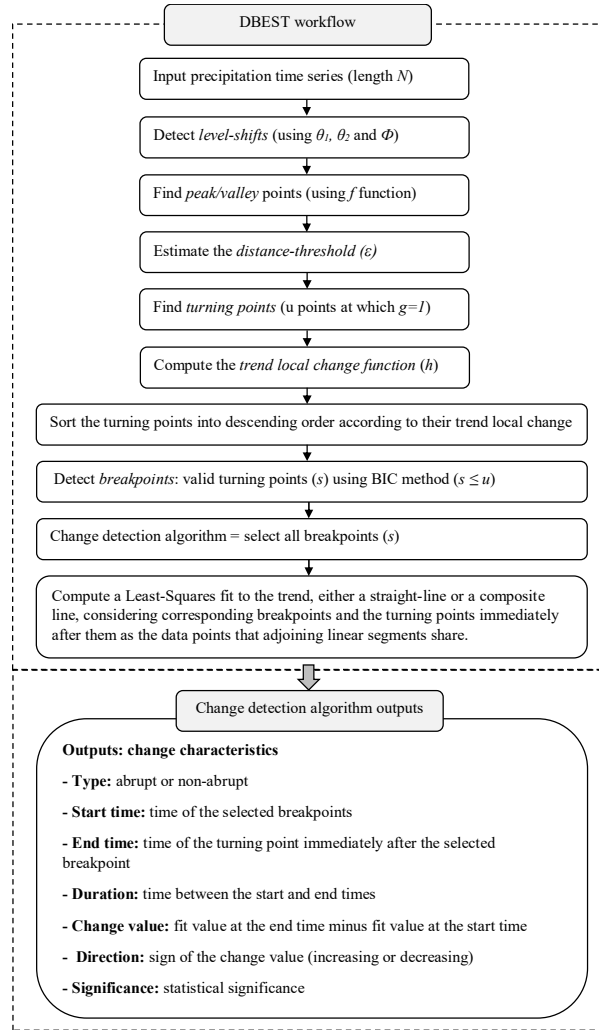


Figure 1. Flowchart of DBEST algorithm for detecting and characterizing changes in pixel-based precipitation dataset (after Jamali et al. [25]).

2.2.2. Data preprocessing

Due to the large spatiotemporal variation in the global precipitation data (month-to-month and region-to-region), it is necessary to provide a meaningful measure of the interannual precipitation changes globally while preserving the relative difference of the observed precipitation at the pixel level. To remove erroneous effects of scale differences on the change detection computation, we applied a pixel-based precipitation time series filter that accounts for two conditions. These conditions disregard the precipitation changes of less than 1mm and 0.05 median value over the study period. For ex-

228

229

230

231

232

233

234

235

236

237

238

239

ample, the precipitation changes of 10 to 20% for the recorded event of below 1 mm may mathematically be considered significant while in the conceptual interpretation this change does not represent a significant abrupt change or a breakpoint in the precipitation time series.

Accordingly, the first filter (Eqn. (4)), detects pixels for which the precipitation range over the studied 22-year period is less than 1 mm. Using this filter, the detected pixels are automatically discarded from DBEST analysis using the below formula:

$$R_i = P_{i \max} - P_{i \min} \quad R_i < 1 \text{ mm at each pixel} \quad (4)$$

where P is precipitation (mm), R is the precipitation range during the 22 years (1998–2019), and i is the pixel number.

The second filter (Eqn. (5)) discards the pixels having a precipitation range lower than 0.05 of their median value during the period using the formula below:

$$R_i = P_{i \max} - P_{i \min} \quad R_i < 0.05 \times P_{i \text{ median}} \quad (5)$$

The 0.05 median value was selected based on the Intergovernmental Panel on Climate Change report [54] that suggests a precipitation change from -5 to $+5\%$ between successive years can be classified as ‘No change’. Also, we used the median value instead of the average, as the median is less influenced by precipitation extremes.

2.2.3. Precipitation changes at global, continental, and climate zone scales

We investigated the precipitation breakpoints and compared their characteristics at a quasi-global scale, i.e., start year, duration, magnitude, abrupt and gradual change type. We conducted breakpoint analysis at the continental vs. global scales to obtain insight regarding the change characteristics on land vs. ocean areas. As precipitation changes based on climate zone rather than depending on continental boundaries, we also evaluated our results associated with different climate zones. Here, we used the world map of Köppen–Geiger climate classification to explore the relationship between precipitation breakpoints features and different climate zones. The Köppen–Geiger climate classification was published in 1900 by Wladimir Köppen that was updated by Rudolf Geiger in 1961. In the last version of this classification, five main climate zones at the global scale have been recognized, encompassing (i) warm temperate, (ii) equatorial, (iii) arid, (iv) snow, and (v) polar [55–56]. To find a likely relationship between precipitation variation and abrupt and non-abrupt changes, we also applied the coefficient of variation (CV) for each pixel during the 1998–2019 period. The CV is defined as the ratio of standard deviation and mean.

Note that the greatest change is considered (both decreasing and increasing) in precipitation during the selected period (22 years). Although a longer-period dataset may provide more insight concerning historical changes, we think it is interesting to focus on the recent greatest changes in precipitation over this period.

3. Results

3.1. Global scale

Figure 2 shows the annual 3B43 mean precipitation (mm) and coefficient of variation (CV%) in precipitation over the period studied. Precipitation at the global scale ranged from ~ 1 to more than 5,000 mm in a year. While some portions of North Africa, Central Asia, North and South Pacific Oceans, and the South Atlantic Ocean received less than 100 mm over a year (Fig. 2a), these regions exhibited the highest CV ($>25\%$), indicating a high rate of variability in the annual precipitation (Fig. 2b).

240
241
242
243
244
245
246
247
248
249
250
251
252
253
254
255
256
257
258
259
260
261
262
263
264
265
266
267
268
269
270
271
272
273
274
275
276
277
278
279
280
281
282
283
284
285
286
287
288
289
290
291

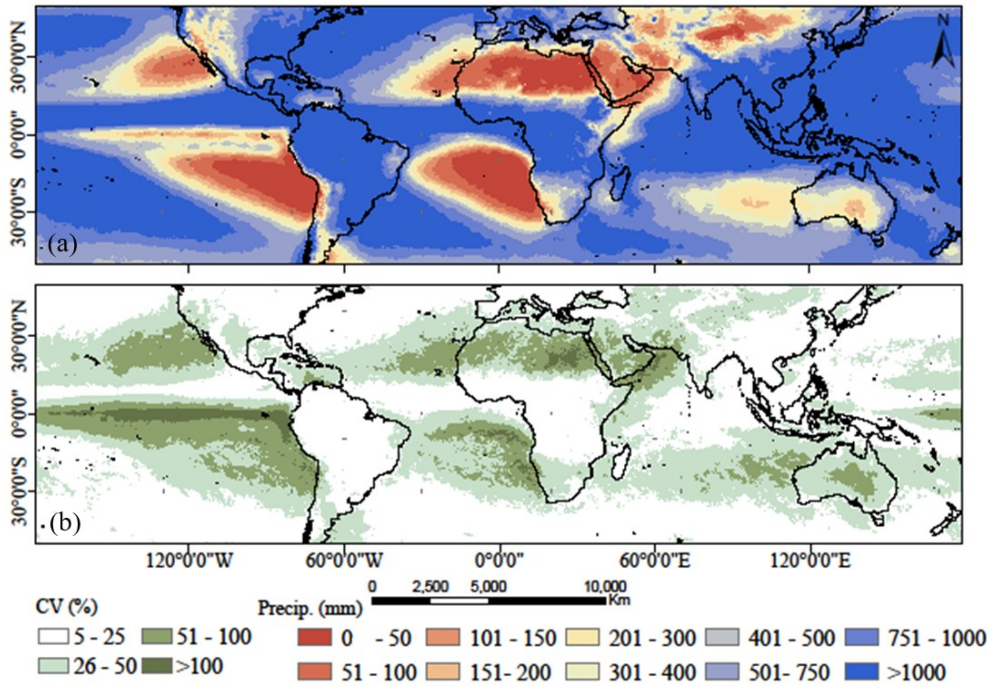


Figure 2. (a) Mean annual precipitation and (b) coefficient of variation, CV, between 1998 and 2019 in 3B43.

Figure 3 depicts the greatest breakpoints detected over the studied period. We found that 14.8% (85,217 pixels) of the entire study area experienced significant changes (abrupt and non-abrupt) in the recorded precipitation (0.05 significance level). An example of a typical abrupt and non-abrupt change in the global precipitation time series is depicted in Fig. 4. In detail, we detected 9.4% non-abrupt changes of which 6.3% occurred over the ocean, 3.1% over land, and 5.4% abrupt changes of which 3.6% occurred over the ocean and 1.8% over land.

The spatial coverage of non-abrupt changes for both ocean and land was considerably higher than abrupt changes (Fig. 3). Most abrupt changes were found near the equator in the Pacific Ocean and Asia relative to other ocean and land regions. Asia, North Africa, South Atlantic, and South Pacific Oceans experienced the highest frequency of breakpoints (abrupt and non-abrupt) in precipitation during the study period compared to the detected breakpoints over Australia, North Pacific, and Atlantic Oceans. Most breakpoints occurred in areas showing high CV > 25% (Fig. 2b and Fig. 3). In contrast, we did not detect many breakpoints in regions with low CV, including regions with high precipitation amounts.

292
293

294
295
296
297
298
299
300
301
302
303
304
305
306
307
308
309
310
311
312
313
314

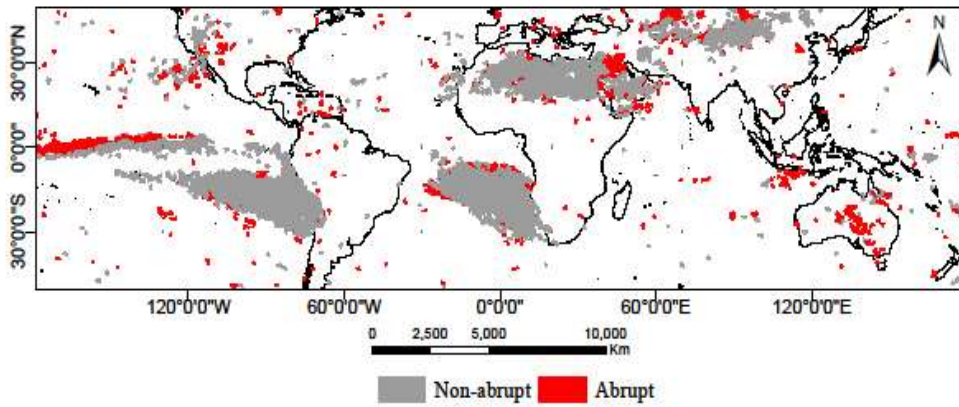


Figure 3. Abrupt and non-abrupt changes in the global precipitation time series, 1998-2019.

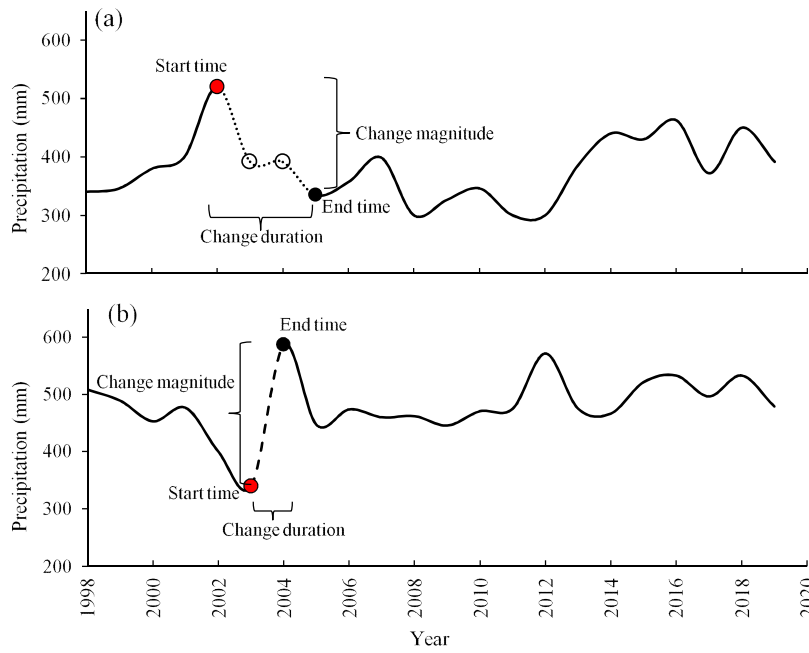


Figure 4. An example of a typical (a) non-abrupt breakpoint with a three-year change duration and -180 mm change magnitude and (b) abrupt breakpoint with a one-year change duration and $+247$ mm change magnitude in the global precipitation time series.

315
316
317
318

319
320
321
322
323

The majority of detected breakpoints, at a global scale, started during 1998, 1999, 2009, 2010, and 2011. Breakpoints in the South Pacific were mainly detected for 1998 and 1999, while in South Atlantic for 2010 and 2011 (Fig. 5). In overland areas, the breakpoints varied from 1998 to 2017.

324
325
326
327
328

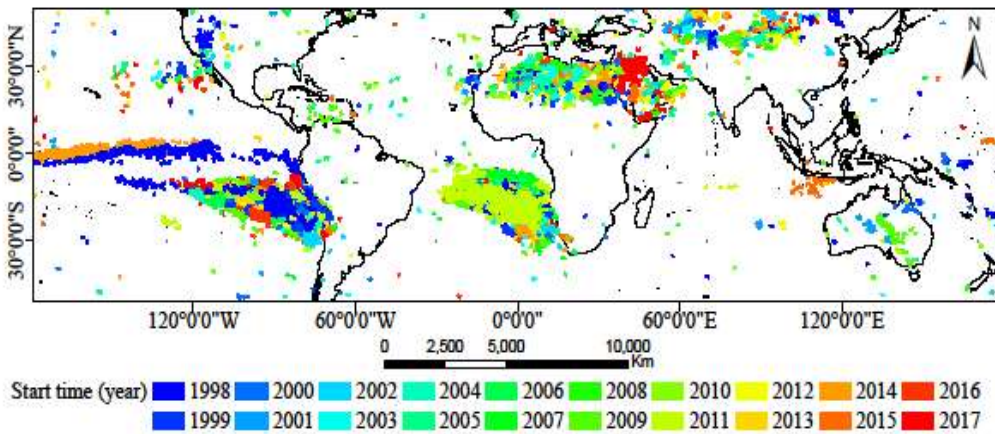


Figure 5. Start time of the breakpoints in the pixel-based global precipitation time series (1998-2019).

329

Figure 6 shows the change duration results (year) at the global scale. Most of the detected breakpoints, 73%, occurred during a relatively short (one-year) period. About 16.8 and 7% of breakpoints occurred during a two- and three-year period, respectively. The remaining percentage, 3.2%, varied between four to nine years.

330
331
332
333
334
335

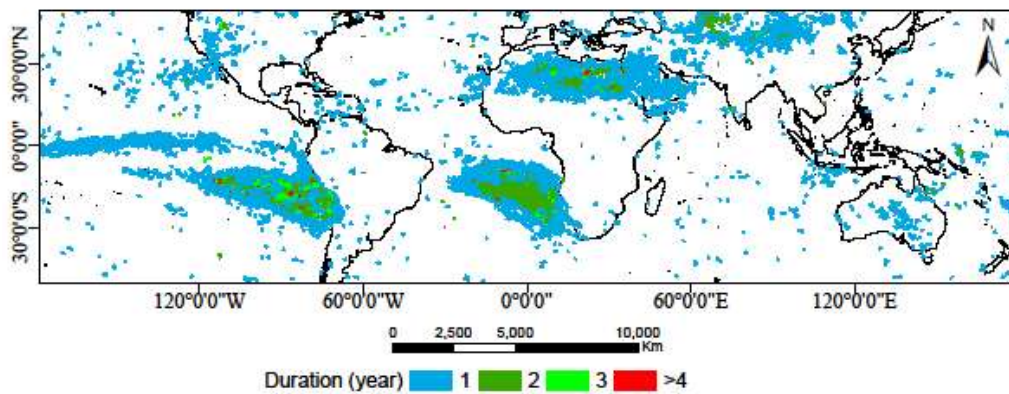


Figure 6. Duration (year) of the abrupt and non-abrupt changes in the global precipitation time series (1998-2019).

336
337
338
339
340
341

The magnitude of precipitation changes varied from -3000 to $+3000$ mm across the globe (Fig. 7). The largest magnitudes were more related to ocean climate, especially near the equator of the Pacific Ocean (± 2000 to ± 3000 mm). Although the precipitation in some regions changed by ± 3000 mm, most changes were about ± 100 mm for the detected breakpoint duration. For instance, precipitation in most portions of Africa and Asia changed with a magnitude of $+100$ mm, including both abrupt and non-abrupt changes. In contrast, most changes over the South Pacific and South Atlantic Oceans occurred with a magnitude of -100 mm (Fig. 7).

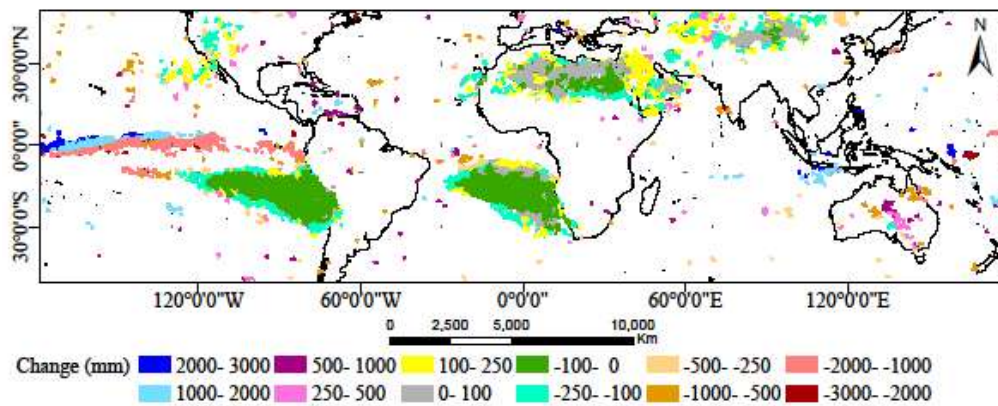


Figure 7. The magnitude of abrupt and non-abrupt changes in the global precipitation time series (1998–2019).

3.2. Continental scale

Significant abrupt and non-abrupt changes over the continents are depicted in Fig. 8a. More significant breakpoints occurred over Africa (23.9%), Asia (22.9%), and Australia (15.4%) as compared to North America (11.6%), South America (9.3%), Europe (8.3%), and Oceania (9.6%). Further, there were more non-abrupt changes in Asia (13.7%) and Africa (18.3%) were more than abrupt changes (Asia: 9.1% and Africa: 5.6%) (Fig. 3). Conversely, the percentage of abrupt changes occurring in Australia (10.4%) was more than that of non-abrupt changes (4.9%). In Africa, a majority of significant breakpoints occurred over the northern region of the continent while in Asia it occurred in the western and central regions of the continent. In North and South America, significant breakpoints mainly extended over western regions of the continent (Fig. 3).

Figure 8b shows the distribution of detected breakpoint occurrences for all continents over the study period. The results indicated that all detected breakpoints extended from 1998 through 2017. This means that we observed no breakpoints for 2018 and 2019. The detected breakpoints only extended during less than 25% of each year except in Australia and Europe, where the breakpoints extended to 37.4 (during 2009) and 30.3% (during 2010), respectively. During 2009 and 2010, South America and Oceania also showed a high percentage of breakpoints relative to other continents. In the first year (1998), North America and Oceania had the highest proportion of breakpoints relative to other continents extending over 23.1 and 20.7% of the year, respectively.

342
343
344
345
346
347
348
349
350

351
352
353
354
355
356
357
358
359
360
361
362
363
364
365
366
367
368
369
370
371
372
373
374
375
376
377

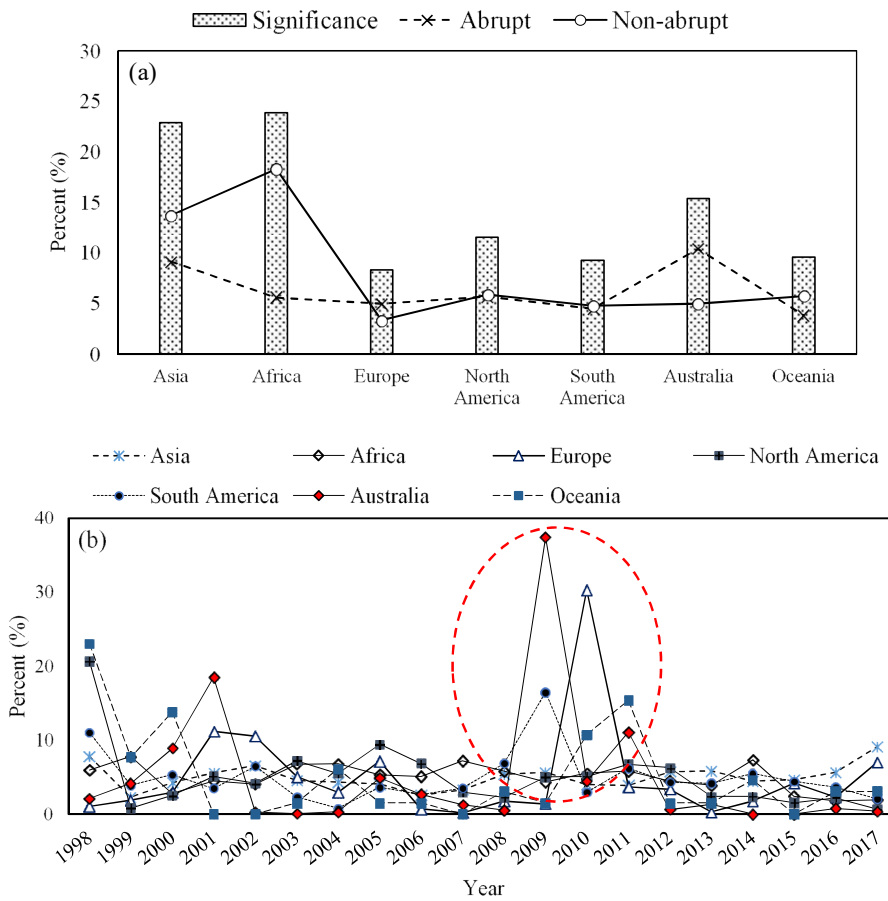


Figure 8. (a) Distribution of all significant breakpoints (column) and abrupt and non-abrupt changes (lines) over different continents and (b) distribution of all significant breakpoints over the 1998-2019 period.

Results for significant positive and negative breakpoints over different continents are given in Table 2. The highest percentage of negative changes (abrupt and non-abrupt) was detected in Oceania (73.8%), Europe (61.8%), North America (56.2%), and South America (55.5%), while the lowest percentage was detected in Asia (41.7%) and Australia (46.9%). Asia, North Africa, and North and South America varied from -100 to +100 mm regarding the magnitude of change. The change value in Australia ranged from -1,000 to +500 mm over the study period (Fig. 7).

378

379
380
381
382
383
384
385
386
387
388
389
390
391
392
393
394

Table 2. Percentage of significant positive (Pos.) and negative (Neg.) breakpoints of precipitation on different continents.

Continent	Asia		Africa		Europe		N. America		S. America		Australia		Oceania	
	Neg.	Pos.	Neg.	Pos.	Neg.	Pos.	Neg.	Pos.	Neg.	Pos.	Neg.	Pos.	Neg.	Pos.
1998	7.1	0.8	3.5	2.5	0.0	1.1	20.5	0.2	6.0	5.1	0.1	2.0	13.8	9.2
1999	1.3	1.1	6.2	1.7	1.6	0.4	0.6	0.2	2.4	1.5	1.8	2.3	4.6	3.1
2000	0.9	3.4	1.8	1.1	0.4	2.6	0.9	1.6	4.0	1.3	8.9	0.0	13.8	0.0
2001	0.4	5.3	1.3	3.3	8.1	3.2	2.6	2.5	2.7	0.8	18.5	0.0	0.0	0.0
2002	1.3	5.3	1.2	2.8	9.8	0.7	0.6	3.5	4.8	1.7	0.0	0.3	0.0	0.0
2003	4.2	0.3	1.6	5.2	0.0	5.1	0.1	7.1	0.4	1.9	0.0	0.1	0.0	1.5
2004	1.7	2.7	2.3	4.5	3.0	0.0	2.9	2.6	0.4	0.4	0.4	0.0	6.2	0.0
2005	2.8	1.3	2.1	3.2	1.2	6.0	7.4	2.0	0.2	3.5	1.3	3.6	0.0	1.5
2006	0.9	1.7	4.3	0.8	0.7	0.0	1.8	5.1	2.2	0.4	1.3	1.3	1.5	0.0
2007	2.3	1.0	3.3	3.9	0.0	0.2	1.2	1.8	1.7	1.8	0.1	1.2	0.0	0.0
2008	1.4	4.1	3.4	2.4	0.0	1.8	1.9	0.4	5.6	1.2	0.0	0.5	3.1	0.0
2009	1.2	4.5	2.8	1.6	0.5	0.9	1.9	3.1	8.1	8.4	0.1	37.4	0.0	1.5
2010	2.5	1.5	3.2	2.4	30.4	0.0	3.2	1.9	0.4	2.5	1.6	2.9	9.2	1.5
2011	0.8	3.0	1.1	4.7	0.4	3.3	5.8	1.0	4.6	1.6	11.1	0.0	15.4	0.0
2012	2.4	3.4	3.8	0.7	1.8	1.6	1.3	5.0	3.0	1.3	0.6	0.1	1.5	0.0
2013	2.7	3.2	1.3	2.6	0.2	0.2	0.1	2.3	1.9	2.3	0.0	1.3	1.5	0.0
2014	0.9	3.5	4.4	3.0	1.6	0.2	0.2	2.2	4.1	1.4	0.0	0.0	3.1	1.5
2015	1.8	2.9	1.7	0.7	0.0	4.2	0.8	0.7	1.3	3.1	0.0	0.0	0.0	0.0
2016	5.1	0.6	0.5	1.3	2.3	0.0	1.9	0.3	0.4	3.3	0.7	0.1	0.0	3.1
2017	0.3	8.8	0.2	1.7	0.0	7.0	0.4	0.3	1.2	0.8	0.4	0.0	0.0	3.1
Total	41.7	58.3	50.0	50.0	61.8	38.2	56.2	43.8	55.5	44.5	46.9	53.1	73.8	26.2
Average	2.1	2.9	2.5	2.5	3.1	1.9	2.8	2.2	2.8	2.2	2.3	2.7	3.7	1.3

3.3. Climate zone scale

We observed that the most significant breakpoints occurred in arid (31.6%) and polar (24.1%) climates while we found fewer breakpoints' events in snow-covered areas (11.5%), equatorial (7.5%), and warm temperate (7.7%) climate zones (Fig. 9a). The results of the change type indicated that the non-abrupt changes in arid (abrupt: 9.8%; non-abrupt: 21.7%) and polar (abrupt: 10.2%; non-abrupt: 13.9%) climates extended over a larger area compared to snow-covered regions (abrupt: 5.1%; non-abrupt: 6.4%), equatorial (abrupt: 4.4%; non-abrupt: 3.1%), and warm temperate (abrupt: 4.5%; non-abrupt: 3.2%) climate zones (Fig. 9a). Figure 9b shows the breakpoint year for different climate zones. In principle, the results obtained for the start time indicated that breakpoints only occurred from 1998 to 2017 in different climate zones (Fig. 9b) with about 10% for each year in all climate zones except equatorial and snow climates, which indicated a higher percentage (~17.5%) in 1998 and 2009 (Figs. 10a and b). The results of durations revealed that most of the detected breakpoints (>85%) occurred over a one- to two-year period in different climate zones.

395
396397
398
399
400
401
402
403
404
405
406
407
408
409
410
411
412
413

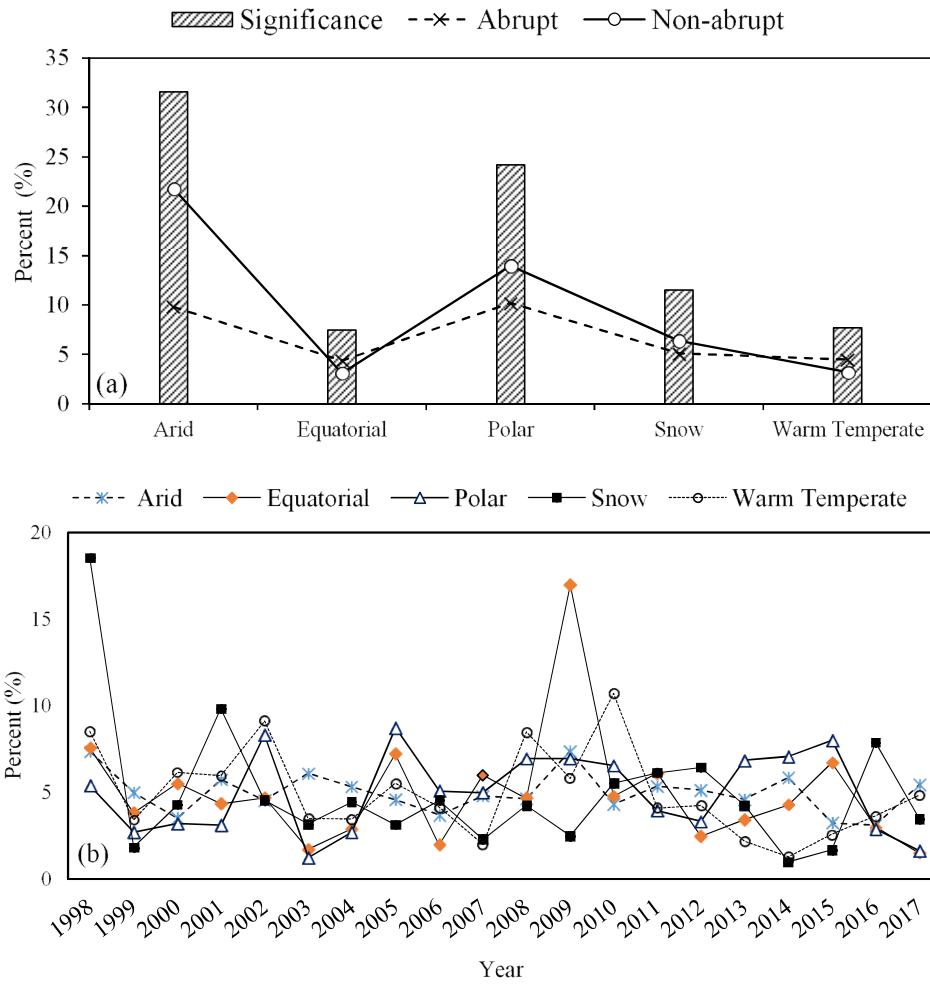


Figure 9. (a) Distribution of all significant breakpoints (column) and abrupt and non-abrupt changes (lines) in different climate zones and (b) distribution of all significant breakpoints over the 1988-2019 period.

414

415

416

417

418

419

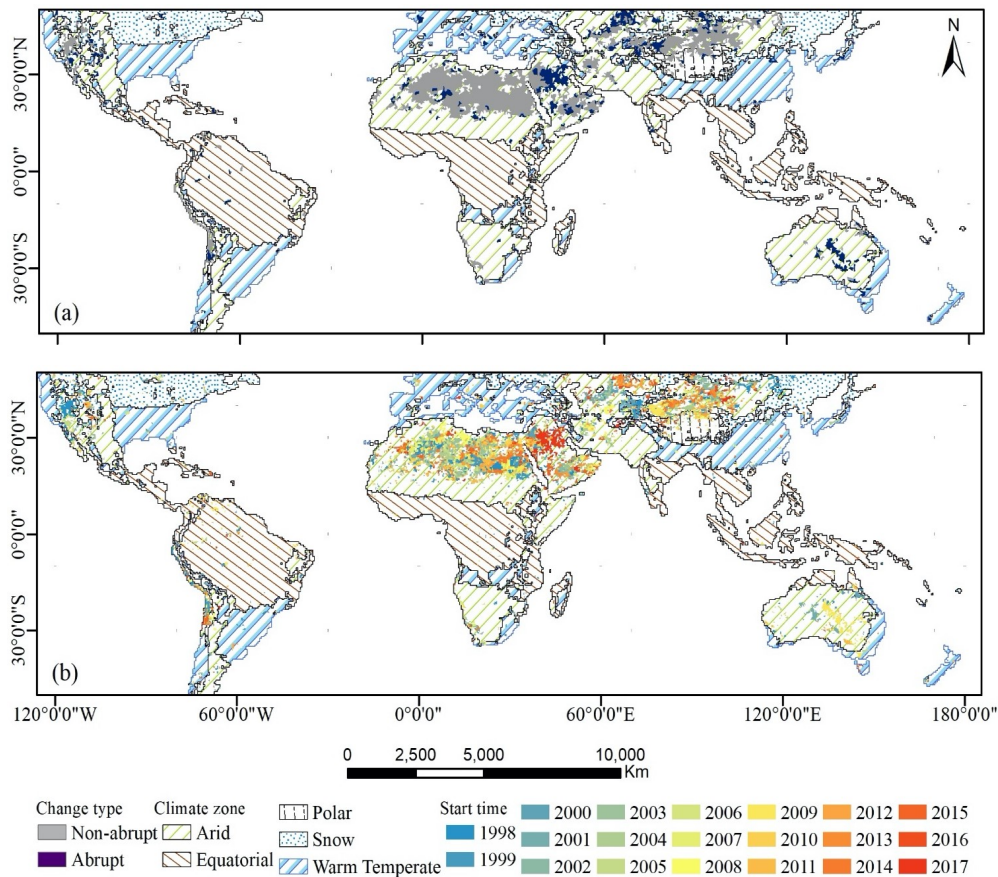


Figure 10. (a) Abrupt and non-abrupt changes at 0.05% significance level and (b) their start time, in different climate zones over the 1998-2019 period.

We detected higher percentages of positive breakpoints in arid (54%) and equatorial (51.9%) climates relative to those in other climate zones. Further, the highest percentage of negative breakpoints was found over the polar, snow-covered, and warm temperate climates with about 55% each relative to other climate zones (Table 3).

According to Table 4, positive changes ranged from 3 to 2,720 mm per year (on average 164 mm), while negative changes varied from -2,114 to -3 mm per year (on average -174 mm) in the arid climate. The mean of positive and negative changes specified that most changes were lower than ± 180 mm per year in the arid climate zone over the study period. Similarly, the average detected precipitation changes in the polar climate were 194 mm and -159 mm per year for the positive and negative changes, respectively. We found the greatest change in the equatorial climate zone with a mean of 874 mm and -847 mm per year (variation from 3,000 to -2,998 mm) for positive and negative changes, respectively. The mean change for the snowy climate zone was +326 mm and -324 mm for the positive and negative changes, respectively. We found 574 mm and -634 mm of pos-

420

421

422

423

424

425

426

427

428

429

430

431

432

433

434

435

436

437

438

itive and negative precipitation changes per year in the warm temperate climate zone, respectively (Table 4).

Table 3. Percentage of significant positive (Pos.) and negative (Neg.) breakpoints in precipitation for different climate zones.

Climate Year	Arid (%)		Equatorial (%)		Polar (%)		Snow (%)		Warm Temperate (%)	
	Neg.	Pos.	Neg.	Pos.	Neg.	Pos.	Neg.	Pos.	Neg.	Pos.
1998	5.9	1.5	1.6	6.0	3.6	1.8	18.1	0.5	7.8	0.8
1999	3.5	1.5	2.5	1.4	2.1	0.6	1.7	0.2	2.4	1.0
2000	1.6	1.9	4.7	0.9	2.3	0.9	2.2	2.2	2.4	3.8
2001	2.1	3.6	3.0	1.4	0.9	2.2	4.3	5.6	2.2	3.8
2002	1.0	3.5	2.0	2.7	3.5	4.8	1.4	3.2	5.5	3.7
2003	2.8	3.3	0.5	1.2	0.8	0.4	1.3	2.0	0.9	2.6
2004	1.9	3.5	1.0	1.9	0.3	2.4	1.7	2.8	3.3	0.2
2005	2.7	1.9	0.8	6.5	7.7	1.0	2.2	1.0	2.8	2.7
2006	2.7	1.1	1.1	0.9	0.8	4.3	1.0	3.6	1.7	2.5
2007	2.4	2.4	4.4	1.6	2.1	2.9	0.6	1.8	1.0	1.1
2008	2.0	2.7	3.9	0.8	3.9	3.1	0.7	3.6	4.7	3.8
2009	1.9	5.5	6.4	10.5	1.6	5.4	1.3	1.2	1.2	4.6
2010	2.6	1.8	1.9	2.9	4.2	2.4	3.3	2.3	8.4	2.3
2011	1.9	3.4	4.4	1.8	2.8	1.1	3.9	2.3	1.9	2.2
2012	2.7	2.4	1.8	0.7	2.4	0.9	1.7	4.8	3.5	0.7
2013	1.6	3.0	2.8	0.6	4.3	2.6	2.0	2.3	0.7	1.5
2014	2.4	3.5	3.2	1.1	5.3	1.8	0.3	0.8	0.7	0.6
2015	1.6	1.7	1.3	5.4	3.8	4.3	0.4	1.3	1.1	1.5
2016	2.4	0.7	0.2	2.8	1.5	1.5	7.5	0.5	2.2	1.4
2017	0.3	5.1	0.6	0.9	1.0	0.6	0.3	3.2	0.5	4.4
Total	46.0	54.0	48.1	51.9	54.9	45.1	55.4	44.7	55.0	45.1
Average	2.3	2.7	2.4	2.6	2.7	2.3	2.8	2.2	2.7	2.3

Table 4. Statistical description of precipitation changes in different climate zones.

Climate Change (mm)	Arid		Equatorial		Polar		Snow		Warm Temperate	
	Pos.	Neg.	Pos.	Neg.	Pos.	Neg.	Pos.	Neg.	Pos.	Neg.
Mean	164.0	-174.3	874.4	-846.8	194.2	-159.5	326.4	-323.7	574.5	-634.3
Max	2719.6	-2.9	3122.1	-223.0	1074.2	-57.4	981.9	-98.6	4967.6	-126.9
Min	3.2	-2113.6	198.0	-2998.4	57.7	-1348.0	88.9	-1547.0	116.5	-2801.8

4. Discussion

4.1. Precipitation changes at global scale

Due to the great loss of human lives and exponentially increasing damage costs associated with extreme precipitation events, studying abrupt and non-abrupt changes in precipitation has received much attention in recent years [57] because they provide insight as to how climate extremes influence the ecosystem and society [57]. Also, as the spatial distribution of precipitation is not limited to a particular region with a defined geopolitical boundary such as cities, countries, and continents, it is necessary to conduct research considering spatial aggregation representing different climatological characteristics.

The CV is robust in detecting precipitation variability and changes [58]. Also, significant deviations from mean annual precipitation (i.e., high CV) can significantly stress to ecological and human systems [59]. Generally, high temporal variability in precipitation (month to month and year to year) is the leading cause of the detected changes. For instance, some portions of North Africa, Central Asia, the North and South Pacific Oceans, and the South Atlantic Ocean receive precipitation lower than 100 mm/year. At the same time, these regions have the highest CV (more than 25%). In addition, precipitation variability can increase over time. Dore [60] reported increased precipitation variance globally, with higher variability over the equatorial region.

On the global scale, the detected breakpoints in precipitation can be derived from significant shift changes with decreasing light precipitation and increasing heavy precipitation over time. Recently, researchers have reported that light precipitation events significantly decreased during past decades on regional and global scales (e.g., [61–64]). For instance, Ma et al. [62] reported that very heavy precipitation ($P \geq 50 \text{ mm day}^{-1}$) events have increased significantly from 1960 to 2013, while light ($0.1 \leq P < 10 \text{ mm day}^{-1}$) and moderate ($10 \leq P < 25 \text{ mm day}^{-1}$) events have decreased significantly in China. This indicates a shift from light to intense precipitation, implying increased risks of drought and floods [62]. As well, increasing heavy precipitation events can cause significant abrupt and non-abrupt changes in precipitation. It is noteworthy to clarify that the abrupt and non-abrupt changes in precipitation can also be due to various local and regional natural and human impacts, including changes in the environment, measurement techniques, observation locations, and equipment [12].

Our findings indicated that most of the detected breakpoints, abrupt and non-abrupt changes, occurred over the land area in the Northern Hemisphere. In contrast, in the Southern Hemisphere, they occurred over the oceans. The most significant breakpoints in the Northern Hemisphere were found over Asia and North Africa (dry regions). In contrast, the highest percentage of breakpoints in the Southern Hemisphere was detected near the Equator in the South Pacific and South Atlantic, wet regions. Most breakpoints occurred in areas with low precipitation and high CV, which could be due to internal and external environmental factors. Conversely, we found no significant breakpoints in regions with low CV (including regions with high precipitation). This means that some dry regions (i.e., North Africa and Asia) and wet regions (i.e., South Pacific and South Atlantic) with high CV showed significant breakpoints in precipitation that can be expected to experience more extreme events due to climate change and this intensification can lead to increased risk of floods, soil erosion, and droughts [64].

Although there is considerable variability in spatial trend patterns, observations suggest that the number of extreme precipitation events has increased globally (e.g., [4, 6, 9, 65]), hence generating the greatest changes in precipitation. We found a high number of breakpoints during 1998–1999 and 2009–2011 across the globe. Over the South Pacific Ocean, we detected more breakpoints in 1998 and 1999 while in the South Atlantic similar number of breakpoints was found in 2010 and 2011. A warmer tropical Pacific in 1998 was caused by a positive El Niño Southern Oscillation (ENSO) event [60]. ENSO influences precipitation changes at the global scale [66–70] and is related to the variations of temperature and precipitation over much of the sub-tropics and tropics, as well as some mid-latitude regions [60]. In line with the detected breakpoint years related to ENSO, a global increase in surface temperature for El Niños (1998 and 2010) and negative global anomalies during La Niñas (1999–2001) have been reported. The maximum amplitude of surface temperature occurred during the 1998 El Niño ($\sim +0.15 \text{ }^\circ\text{C}$), with a lower amplitude (negative) during La Niña, 1999–2001. Moreover, during the cold (warm) phase of ENSO, La Niña (El Niño), most of the tropical ocean surfaces are cooler (warmer) than normal, and the atmosphere is charged with less (more) moisture, resulting in less (more) extreme precipitation events over the (combined ocean and land) tropical region [66, 69]. Higher surface temperature leads to a greater evaporation rate (especially over the ocean and overtime) and a greater instability; hence, impacting the variation of large-scale pre-

465
466
467
468
469
470
471
472
473
474
475
476
477
478
479
480
481
482
483
484
485
486
487
488
489
490
491
492
493
494
495
496
497
498
499
500
501
502
503
504
505
506
507
508
509
510
511
512
513
514
515
516
517
518

precipitation [3]. Lausier and Jain [59] reported that sea surface temperature variability patterns were strongly correlated with global precipitation patterns during 1951–2011 helping to drive variability in annual precipitation. Adler et al. [3] stated that the ocean shows the opposite anomaly compared to the land areas for ENSO.

Regarding the large El Niño during 1998, positive and negative anomalies occurred over the ocean and land areas, respectively. This is due to the pattern of positive rainfall anomalies over the tropics, particularly the central and eastern Pacific Oceans, which could be a reason for the detected breakpoints in the land regions versus ocean areas in our study. These reported results, along with our findings have already been addressed in both climate simulations and satellite observations [66, 69], indicating that ENSO is a dominant driver of precipitation extremes in the tropics [69].

Our findings indicate that the change in magnitude of precipitation notably occurred over the oceans, especially near the Equator in the Pacific Ocean. Analyses of the Climate Prediction Center (CPC) Merged Analysis of Precipitation (CMAP) product [71] and the National Centers for Environmental Prediction (NCEP) reanalysis project [72] show that there have been substantial increases in average precipitation over the tropical oceans, related to increased intensity and frequency of ENSO during 1979–1998 [2]. Similarly, we found a substantial spatial coverage of breakpoints, abrupt and non-abrupt, occurring over Asia, North Africa, South Atlantic, and South Pacific Oceans. Moreover, the detected breakpoints revealed that a decreasing precipitation trend impacted some parts of the subtropics and tropics compared to other regions. Likewise, Trenberth et al. [73] reported a noticeable change in precipitation pattern in recent years, suggesting a wetter condition for the high latitudes and a drier condition for the subtropics and tropics, which is associated with the large-scale precipitation change influenced by ENSO [74]. Further, our findings indicated that the Indian and North Atlantic Oceans experienced the lowest number of breakpoint occurrences in precipitation over the study period. This is contrary to findings by Pokhrel et al. [75] who used Objectively Analyzed air-sea Fluxes (OAF flux) and the latest version of National Centers for Environment Prediction (NCEP) Climate Forecast System (CFS) version-2 products. They reported significant precipitation variability and changes over the Indian Ocean affected by El Niño and La Niña signals during the earlier period 1979–2010, which partially overlaps the period of the current study. This contradiction could be due to the usage of several variables such as evaporation-precipitation (E-P), wind speed, air-sea humidity, and sea surface temperature (SST), which was different from the only precipitation variable used in this study. The past time series (<1998) were not available, but the changes in precipitation between 1998 and 1999 and subsequent years (>1999) were abrupt, which were considered breakpoints in our study. More importantly, the detected breakpoints during 1998–1999 were more reasonable than other years' changes due to the reported substantial increases in average precipitation over the tropical oceans, related to increased intensity and frequency of ENSO during 1979–1998 [2].

4.2. Precipitation changes at the continental and climate scales

We detected a higher frequency of breakpoints over Africa, Asia, and Australia relative to other continents. Not only the spatial coverage of non-abrupt changes for both ocean and land was considerably higher than abrupt changes but also the detected non-abrupt changes in Asia and Africa were more than that of abrupt changes. This means that the magnitude of precipitation changes in these regions was low. Although we found a large number of breakpoints over some regions of Asia and Africa, we detected the lowest changes in the magnitude of precipitation (± 100 mm), which is due to the high CV in these regions (i.e., low precipitation amount but high precipitation variability). These breakpoints could be related to the observed extreme rainfall events, especially over north tropical Asia, around 10–20° N, [76].

Major precipitation and severe drought occurrences can be related to positive and negative breakpoints, respectively. Frequent severe drought and flood events, especially

519
520
521
522
523
524
525
526
527
528
529
530
531
532
533
534
535
536
537
538
539
540
541
542
543
544
545
546
547
548
549
550
551
552
553
554
555
556
557
558
559
560
561
562
563
564
565
566
567
568
569
570
571
572

in the central region of Asia, during the past decades, have been reported [64, 67], which agrees with the spatial distribution of the detected breakpoints over Asia in this study. Moreover, an increase of 1.3°C in average temperature over Asia, particularly China, with increased evaporation has led to extreme regional precipitation and observed breakpoints (e.g., [77-80]). In North and South America, we found significant breakpoints extending over western regions of the continents. The changes in extreme precipitation and duration are likely to result from the combined effects of large-scale circulation changes and climate change. Climate change may affect the probability and intensity of extreme weather events [66, 78], as it can be the main reason for breakpoints in precipitation.

Regarding climate zones, we found that the majority of significant breakpoints occurred over the arid and polar climates relative to other climate zones. Our findings indicate that detected breakpoints in precipitation over the arid climate were mainly positive (upward) compared to other climate zones (i.e., Asia and Africa). To address this observation, it is noted that the arid climate is characterized by limited precipitation with a high spatial and temporal variation that explains the higher density of the detected breakpoints over this zone [81-83]. The change in the average precipitation in arid climates specified that the majority of breakpoints were detected in the range between -180 and +180 mm over the studied period. Conversely, we found minor breakpoints in the equatorial and warm temperate (<8%) climate zones. The equatorial climate mainly covers central Africa, northern regions of South America, southern India, Sri Lanka, northern Australia, Indonesia, Thailand, Vietnam, Malaysia, Laos, Philippines, Myanmar, and most Pacific Island nations based on the climate classification scheme. It seems that the equatorial climate with a high humidity regime provides a low variability, which can be the main reason for detecting fewer breakpoints. For example, the equatorial climate of Central Africa sustains tropical rainforests throughout the region and provides the excellent growing conditions needed for high-value crops [84].

Our findings indicate that high precipitation variability is the leading cause of significant breakpoints. Precipitation variability is a crucial climatic factor for the environment, agriculture, and society. Increased precipitation variability can reduce agricultural yield [85] and affect the development [86-87]. This connects extreme dry and wet events, droughts, and floods, posing threats to the society and environment [86, 88]. Much more attention needs to be given to regions with many abrupt changes to mitigate the impact of extreme natural events such as droughts and floods derived from climate extremes. Therefore, this study provides essential information to pinpoint the areas under frequent precipitation changes at the quasi-global and continental scales and their associations with the climate zones. Finally, theoretical and practical research is required to connect the understanding of changes in precipitation, and the threats they pose to the environment and society.

5. Conclusions

To decrease the impacts of floods and droughts, there is a vital need to study historical events, i.e., breakpoints in precipitation, at the global scale. Although there are several studies concerning precipitation changes, breakpoints, and trends, on a regional scale using common statistical tests, conducting a comprehensive global investigation on the greatest changes in precipitation is of great importance. We used the DBEST algorithm for analyzing precipitation change and its characteristics in a monthly satellite-based precipitation dataset (TRMM 3B43) at three different scales (i) global, (ii) continental, and (iii) climate zone over the 1998-2019 period. Unlike previous studies on precipitation changes at the local and regional scales, this study focused on quasi-global scale precipitation to detect general patterns of both abrupt and non-abrupt changes. This helps better understand the changes in overall precipitation patterns and adequately develop a mitigation strategy for future likely extreme event impacts.

573
574
575
576
577
578
579
580
581
582
583
584
585
586
587
588
589
590
591
592
593
594
595
596
597
598
599
600
601
602
603
604
605
606
607
608
609
610
611
612

613
614
615
616
617
618
619
620
621
622
623
624
625

The output of the DBEST algorithm captured the type (non-abrupt or abrupt) and characteristics (magnitude and time) of the significant breakpoints observed in satellite-based precipitation time series. We found 14.1% abrupt and non-abrupt significant breakpoints in the quasi-global precipitation dataset (0.05 significance level). The highest percentage of abrupt changes was found near the equator in the Pacific Ocean and Asia relative to other oceans and land regions. On the continental scale, the detected breakpoints in Africa (23.9%), Asia (22.9%), and Australia (15.4%) were more than those in North America (11.6%), South America (9.3%), Europe (8.3%) and Oceania (9.6%). The findings indicated that the most significant breakpoints were found in the arid (31.6%) and polar (24.1%) climates on the climate zone scale. The detected breakpoints in precipitation are more likely to be related to the extreme wet and dry events associated with ENSO and high precipitation variability. However, these results indicated that abrupt changes in precipitation differ not only between regions but also in different aspects of precipitation, i.e., total and extreme.

The consequences of precipitation variability and change, substantial changes, affect water resources at the local to regional scale where crops are grown, people live, and industrial and agricultural water requirements for production purposes exist. Our findings indicate that larger parts of Africa and Asia experienced a significant number of the most extensive changes in precipitation. Compared to the average state (trend during a specific period), the greatest changes in precipitation in these regions were more abrupt which may pose a severe threat to the ecology, environment, and natural resources causing a substantial loss in urban and rural areas.

In conclusion, this study provides a large-scale comprehensive perspective of abrupt and non-abrupt precipitation changes over the global, continental, and climate zone during the 1998–2019 period. The monthly satellite pixel-based precipitation dataset (TRMM 3B43) provided valuable information to address the precipitation change characteristics during the last two decades. The DBEST algorithm detected and quantified the major changes in precipitation over large areas at continental and global scales. While applying this algorithm in the precipitation studies, it is suggested that this algorithm be implemented using other climate variables. It is a flexible, accurate, and fast tool for change detection, and is applicable to global change studies using time series of satellite-based datasets.

Author Contributions: Conceptualization, Methodology, Writing-Original draft preparation, Software, Validation, M.K; Conceptualization, Supervision, Methodology, Writing- Reviewing and Editing, H.H; Conceptualization, Methodology, Software, Writing- Reviewing and Editing, S.J; Reviewing and Editing, C.B.U, R.B, and G.J.H. All authors have read and agreed to the published version of the manuscript.

Funding: This research received no external funding.

Data Availability Statement: Data are available from the Tropical Rainfall Measuring Mission (TRMM) datasets. (https://disc.gsfc.nasa.gov/datasets/TRMM_3B43_7/summary).

Acknowledgments: The authors would like to thank the National Aeronautics and Space Administration (NASA) and the Japan Aerospace Exploration Agency (JAXA) for providing the Tropical Rainfall Measuring Mission (TRMM) datasets. The 3B43 data can be downloaded at <https://disc.gsfc.nasa.gov/datasets/TRMM_3B43_7/summary>.

Conflicts of Interest: The authors declare no conflict of interest.

References

1. Longobardi, A.; Villani, P., Trend analysis of annual and seasonal rainfall time series in the Mediterranean area. *International journal of Climatology* **2010**, *30* (10), 1538–1546.

2. Trenberth, K. E., Changes in precipitation with climate change. *Climate research* **2011**, *47* (1-2), 123-138. 677
3. Adler, R. F.; Gu, G.; Sapiano, M.; Wang, J.-J.; Huffman, G. J., Global precipitation: Means, variations and trends during the satellite era (1979–2014). *Surveys in Geophysics* **2017**, *38* (4), 679-699. 678
679
4. Donat, M. G.; Lowry, A. L.; Alexander, L. V.; O’Gorman, P. A.; Maher, N., Addendum: More extreme precipitation in the world’s dry and wet regions. *Nature Climate Change* **2017**, *7* (2), 154-158. 680
681
5. Alexander, L. V.; Zhang, X.; Peterson, T. C.; Caesar, J.; Gleason, B.; Klein Tank, A.; Haylock, M.; Collins, D.; Trewin, B.; Rahimzadeh, F., Global observed changes in daily climate extremes of temperature and precipitation. *Journal of Geophysical Research: Atmospheres* **2006**, *111* (D5). 682
683
684
6. Westra, S.; Alexander, L. V.; Zwiers, F. W., Global increasing trends in annual maximum daily precipitation. *Journal of climate* **2013**, *26* (11), 3904-3918. 685
686
7. Kharin, V. V.; Zwiers, F. W.; Zhang, X.; Wehner, M., Changes in temperature and precipitation extremes in the CMIP5 ensemble. *Climatic change* **2013**, *119* (2), 345-357. 687
688
8. Sillmann, J.; Kharin, V. V.; Zwiers, F.; Zhang, X.; Bronaugh, D., Climate extremes indices in the CMIP5 multimodel ensemble: Part 2. Future climate projections. *Journal of geophysical research: atmospheres* **2013**, *118* (6), 2473-2493. 689
690
9. Donat, M.; Alexander, L. V.; Yang, H.; Durre, I.; Vose, R.; Dunn, R. J.; Willett, K. M.; Aguilar, E.; Brunet, M.; Caesar, J., Updated analyses of temperature and precipitation extreme indices since the beginning of the twentieth century: The HadEX2 dataset. *Journal of Geophysical Research: Atmospheres* **2013**, *118* (5), 2098-2118. 691
692
693
10. Zhang, S. H.; Zhang, P. Y., “Abrupt change study in climate change,” *Advance in Earth Sciences* **1989**, *3*, 47–54. 694
11. Buishand, T., Tests for detecting a shift in the mean of hydrological time series. *Journal of hydrology* **1984**, *73* (1-2), 51-69. 695
12. Reeves, J.; Chen, J.; Wang, X.; Lund, R.; Lu, Q., A review and comparison of climate control data for climate data. *J. Appl. Meteorol. Clim* **2007**, *46*, 900-915. 696
697
13. Zhao, C.; Cui, Y.; Zhou, X.; Wang, Y., Evaluation of performance of different methods in detecting abrupt climate changes. *Discrete Dynamics in Nature and Society* **2016**, 2016. 698
699
14. Lund, R.; Reeves, J., Detection of undocumented changepoints: A revision of the two-phase regression model. *Journal of Climate* **2002**, *15* (17), 2547-2554. 700
701
15. Seidou, O.; Ouarda, T. B., Recursion-based multiple changepoint detection in multiple linear regression and application to river streamflows. *Water Resources Research* **2007**, *43* (7). 702
703
16. Wang, X. L., Comments on “Detection of undocumented changepoints: A revision of the two-phase regression model”. *Journal of Climate* **2003**, *16* (20), 3383-3385. 704
705
17. Worsley, K., On the likelihood ratio test for a shift in location of normal populations. *Journal of the American Statistical Association* **1979**, *74* (366a), 365-367. 706
707
18. Buishand, T. A., Some methods for testing the homogeneity of rainfall records. *Journal of hydrology* **1982**, *58* (1-2), 11-27. 708
19. Pettitt, A. N., A non-parametric approach to the change-point problem. *Journal of the Royal Statistical Society: Series C (Applied Statistics)* **1979**, *28* (2), 126-135. 709
710
20. Alexandersson, H., A homogeneity test applied to precipitation data. *Journal of climatology* **1986**, *6* (6), 661-675. 711
21. Hsu, K.-C.; Li, S.-T., Clustering spatial-temporal precipitation data using wavelet transform and self-organizing map neural network. *Advances in Water Resources* **2010**, *33* (2), 190-200. 712
713
22. Vincent, L. A., A technique for the identification of inhomogeneities in Canadian temperature series. *Journal of Climate* **1998**, *11* (5), 1094-1104. 714
715
23. Kazemzadeh, M.; Malekian, A., Homogeneity analysis of streamflow records in arid and semi-arid regions of northwestern Iran. *Journal of Arid Land* **2018**, *10* (4), 493-506. 716
717
24. McCuen, R. H., *Modeling hydrologic change: statistical methods*. CRC press: 2016. 718

25. Jamali, S.; Jönsson, P.; Eklundh, L.; Ardö, J.; Seaquist, J., Detecting changes in vegetation trends using time series segmentation. *Remote Sensing of Environment* **2015**, *156*, 182-195. 719
26. Schwarz, G., Estimating the dimension of a model. *The annals of statistics* **1978**, 461-464. 720
27. Rousseeuw, P. J.; Leroy, A. M., Robust regression and outlier detection John Wiley & Sons, Inc., New York **1987**. 721
28. Lenderink, G.; Van Meijgaard, E., Increase in hourly precipitation extremes beyond expectations from temperature changes. *Nature Geoscience* **2008**, *1* (8), 511-514. 722
29. O’Gorman, P. A., Sensitivity of tropical precipitation extremes to climate change. *Nature Geoscience* **2012**, *5* (10), 697-700. 723
30. Huffman, G.; Adler, R.; Bolvin, D.; Gu, G.; Nelkin, E.; Bowman, K.; Hong, Y.; Stocker, E.; Wolff, D., The TRMM multi-satellite precipitation analysis: Quasi-global, multi-year, combined sensor precipitation estimates at fine scales. *Journal of Hydrometeorology* **2007**, *8*, 28-55. 724
31. Kummerow, C.; Simpson, J.; Thiele, O.; Barnes, W.; Chang, A.; Stocker, E.; Adler, R.; Hou, A.; Kakar, R.; Wentz, F., The status of the Tropical Rainfall Measuring Mission (TRMM) after two years in orbit. *Journal of applied meteorology* **2000**, *39* (12), 1965-1982. 725
32. Huffman, G. J.; Adler, R. F.; Bolvin, D. T.; Nelkin, E. J., The TRMM multi-satellite precipitation analysis (TMPA). In *Satellite rainfall applications for surface hydrology*, Springer: 2010; pp 3-22. 726
33. Belete, M.; Deng, J.; Wang, K.; Zhou, M.; Zhu, E.; Shifaw, E.; Bayissa, Y., Evaluation of satellite rainfall products for modeling water yield over the source region of Blue Nile Basin. *Science of the Total Environment* **2020**, *708*, 134834. 727
34. Huffman, G. J.; Bolvin, D. T.; Braithwaite, D.; Hsu, K.-L.; Joyce, R. J.; Kidd, C.; Nelkin, E. J.; Sorooshian, S.; Stocker, E. F.; Tan, J., Integrated multi-satellite retrievals for the global precipitation measurement (GPM) mission (IMERG). In *Satellite precipitation measurement*, Springer: 2020; pp 343-353. 728
35. Huffman, G. J.; Bolvin, D. T., TRMM and other data precipitation data set documentation. *NASA, Greenbelt, USA* **2013**, *28* (2.3), 1. 729
36. Huffman, G. J., The transition in multi-satellite products from TRMM to GPM (TMPA to IMERG). *Algorithm Information Document*. Available online: https://docs.eosdis.nasa.gov/public/project/GPM/TMPA-to-IMERG_transition.pdf (accessed on 2 November 2021) **2016**. 730
37. Kazemzadeh, M.; Hashemi, H.; Jamali, S.; Uvo, C. B.; Berndtsson, R.; Huffman, G. J., Linear and Nonlinear Trend Analyzes in Global Satellite-Based Precipitation, 1998–2017. *Earth’s Future* **2021**, *9* (4), e2020EF001835. 731
38. Hashemi, H.; Fayne, J.; Lakshmi, V.; Huffman, G. J., Very high resolution, altitude-corrected, TMPA-based monthly satellite precipitation product over the CONUS. *Scientific data* **2020**, *7* (1), 1-10. 732
39. Hashemi, H.; Nordin, M.; Lakshmi, V.; Huffman, G. J.; Knight, R., Bias correction of long-term satellite monthly precipitation product (TRMM 3B43) over the conterminous United States. *Journal of Hydrometeorology* **2017**, *18* (9), 2491-2509. 733
40. Prat, O. P.; Nelson, B. R., Characteristics of annual, seasonal, and diurnal precipitation in the Southeastern United States derived from long-term remotely sensed data. *Atmospheric research* **2014**, *144*, 4-20. 734
41. Qiao, L.; Hong, Y.; Chen, S.; Zou, C. B.; Gourley, J. J.; Yong, B., Performance assessment of the successive Version 6 and Version 7 TMPA products over the climate-transitional zone in the southern Great Plains, USA. *Journal of Hydrology* **2014**, *513*, 446-456. 735
42. Zhao, T.; Yatagai, A., Evaluation of TRMM 3B42 product using a new gauge-based analysis of daily precipitation over China. *International Journal of Climatology* **2014**, *34* (8), 2749-2762. 736
43. Brown, J. E., An analysis of the performance of hybrid infrared and microwave satellite precipitation algorithms over India and adjacent regions. *Remote Sensing of Environment* **2006**, *101* (1), 63-81. 737
44. Mondal, A.; Lakshmi, V.; Hashemi, H., Intercomparison of trend analysis of multisatellite monthly precipitation products and gauge measurements for river basins of India. *Journal of Hydrology* **2018**, *565*, 779-790. 738
45. Prakash, S.; Mitra, A. K.; Pai, D.; AghaKouchak, A., From TRMM to GPM: How well can heavy rainfall be detected from space? *Advances in Water Resources* **2016**, *88*, 1-7. 739

46. Huang, Y.; Chen, S.; Cao, Q.; Hong, Y.; Wu, B.; Huang, M.; Qiao, L.; Zhang, Z.; Li, Z.; Li, W., Evaluation of version-7 TRMM multi-satellite precipitation analysis product during the Beijing extreme heavy rainfall event of 21 July 2012. *Water* **2013**, *6* (1), 32-44. 761
47. Li, X.-H.; Zhang, Q.; Xu, C.-Y., Suitability of the TRMM satellite rainfalls in driving a distributed hydrological model for water balance computations in Xinjiang catchment, Poyang lake basin. *Journal of Hydrology* **2012**, *426*, 28-38. 762
48. Darand, M.; Amanollahi, J.; Zandkarimi, S., Evaluation of the performance of TRMM Multi-satellite Precipitation Analysis (TMPA) estimation over Iran. *Atmospheric Research* **2017**, *190*, 121-127. 763
49. Javanmard, S.; Yatagai, A.; Nodzu, M.; BodaghJamali, J.; Kawamoto, H., Comparing high-resolution gridded precipitation data with satellite rainfall estimates of TRMM_3B42 over Iran. *Advances in Geosciences* **2010**, *25*, 119-125. 764
50. Moazami, S.; Golian, S.; Hong, Y.; Sheng, C.; Kavianpour, M. R., Comprehensive evaluation of four high-resolution satellite precipitation products under diverse climate conditions in Iran. *Hydrological Sciences Journal* **2016**, *61* (2), 420-440. 765
51. Jamandre, C.; Narisma, G. T., Spatio-temporal validation of satellite-based rainfall estimates in the Philippines. *Atmospheric Research* **2013**, *122*, 599-608. 766
52. Dinku, T.; Ceccato, P.; Grover-Kopec, E.; Lemma, M.; Connor, S.; Ropelewski, C., Validation of satellite rainfall products over East Africa's complex topography. *International Journal of Remote Sensing* **2007**, *28* (7), 1503-1526. 767
53. Tan, M. L., Assessment of TRMM product for precipitation extreme measurement over the Muda River Basin, Malaysia. *HydroResearch* **2019**, *2*, 69-75. 768
54. Houghton, J. T.; Ding, Y.; Griggs, D. J.; Noguer, M.; van der Linden, P. J.; Dai, X.; Maskell, K.; Johnson, C., *Climate change 2001: the scientific basis: contribution of Working Group I to the third assessment report of the Intergovernmental Panel on Climate Change*. Cambridge university press: 2001. 769
55. Kottek, M.; Grieser, J.; Beck, C.; Rudolf, B.; Rubel, F., World map of the Köppen-Geiger climate classification updated. **2006**. 770
56. Rubel, F.; Kottek, M., Observed and projected climate shifts 1901-2100 depicted by world maps of the Köppen-Geiger climate classification. vol. 19, issue 2. *Meteorol.* 771
57. Chen, Y.; Deng, H.; Li, B.; Li, Z.; Xu, C., Abrupt change of temperature and precipitation extremes in the arid region of Northwest China. *Quaternary International* **2014**, *336*, 35-43. 772
58. Sokol Jurković, R.; Pasarić, Z., Spatial variability of annual precipitation using globally gridded data sets from 1951 to 2000. *International journal of climatology* **2013**, *33* (3), 690-698. 773
59. Lausier, A. M.; Jain, S., Diversity in global patterns of observed precipitation variability and change on river basin scales. *Climatic Change* **2018**, *149* (2), 261-275. 774
60. Dore, M. H., Climate change and changes in global precipitation patterns: what do we know? *Environment international* **2005**, *31* (8), 1167-1181. 775
61. Liu, B.; Xu, M.; Henderson, M., Where have all the showers gone? Regional declines in light precipitation events in China, 1960-2000. *International Journal of Climatology* **2011**, *31* (8), 1177-1191. 776
62. Ma, S.; Zhou, T.; Dai, A.; Han, Z., Observed changes in the distributions of daily precipitation frequency and amount over China from 1960 to 2013. *Journal of Climate* **2015**, *28* (17), 6960-6978. 777
63. Wen, G.; Huang, G.; Tao, W.; Liu, C., Observed trends in light precipitation events over global land during 1961-2010. *Theoretical and Applied Climatology* **2016**, *125* (1), 161-173. 778
64. Yang, T.; Li, Q.; Chen, X.; De Maeyer, P.; Yan, X.; Liu, Y.; Zhao, T.; Li, L., Spatiotemporal variability of the precipitation concentration and diversity in Central Asia. *Atmospheric Research* **2020**, *241*, 104954. 779
65. Groisman, P. Y.; Knight, R. W.; Easterling, D. R.; Karl, T. R.; Hegerl, G. C.; Razuvaev, V. N., Trends in intense precipitation in the climate record. *Journal of climate* **2005**, *18* (9), 1326-1350. 780
66. Allan, R. P.; Soden, B. J., Atmospheric warming and the amplification of precipitation extremes. *Science* **2008**, *321* (5895), 1481-1484. 781

67. Gu, G.; Adler, R. F., Precipitation intensity changes in the tropics from observations and models. *Journal of Climate* **2018**, *31* (12), 4775-4790. 803
68. Huang, P.; Xie, S.-P., Mechanisms of change in ENSO-induced tropical Pacific rainfall variability in a warming climate. *Nature Geoscience* **2015**, *8* (12), 922-926. 804
69. Li, X.-F.; Blenkinsop, S.; Barbero, R.; Yu, J.; Lewis, E.; Lenderink, G.; Guerreiro, S.; Chan, S.; Li, Y.; Ali, H., Global distribution of the intensity and frequency of hourly precipitation and their responses to ENSO. *Climate Dynamics* **2020**, *54* (11), 4823-4839. 805
70. Lyon, B.; Barnston, A. G., ENSO and the spatial extent of interannual precipitation extremes in tropical land areas. *Journal of climate* **2005**, *18* (23), 5095-5109. 806
71. Xie, P.; Arkin, P. A., Global precipitation: A 17-year monthly analysis based on gauge observations, satellite estimates, and numerical model outputs. *Bulletin of the American meteorological society* **1997**, *78* (11), 2539-2558. 807
72. Kalnay, E.; Kanamitsu, M.; Kistler, R.; Collins, W.; Deaven, D.; Gandin, L.; Iredell, M.; Saha, S.; White, G.; Woollen, J., The NCEP/NCAR 40-year reanalysis project. *Bulletin of the American meteorological Society* **1996**, *77* (3), 437-472. 808
73. Trenberth, K. E.; Jones, P. D.; Ambenje, P.; Bojariu, R.; Easterling, D.; Tank, A. K.; Parker, D.; Rahimzadeh, F.; Renwick, J. A.; Rusticucci, M., Observations: surface and atmospheric climate change. In *Climate Change 2007: The Physical Science Basis. Contribution of Working Group 1 to the 4th Assessment Report of the Intergovernmental Panel on Climate Change*, Cambridge University Press: 2007. 809
74. Trenberth, K. E.; Caron, J. M., The Southern Oscillation revisited: Sea level pressures, surface temperatures, and precipitation. *Journal of Climate* **2000**, *13* (24), 4358-4365. 810
75. Pokhrel, S.; Rahaman, H.; Parekh, A.; Saha, S. K.; Dhakate, A.; Chaudhari, H. S.; Gairola, R. M., Evaporation-precipitation variability over Indian Ocean and its assessment in NCEP Climate Forecast System (CFSv2). *Climate Dynamics* **2012**, *39* (9), 2585-2608. 811
76. Matilla, B. C.; Mapes, B. E., A Global Atlas of Tropical Precipitation Extremes. In *Tropical Extremes*, Elsevier: 2019; pp 1-13. 812
77. Dai, A., Increasing drought under global warming in observations and models. *Nature climate change* **2013**, *3* (1), 52-58. 813
78. He, B.-R.; Zhai, P.-M., Changes in persistent and non-persistent extreme precipitation in China from 1961 to 2016. *Advances in Climate Change Research* **2018**, *9* (3), 177-184. 814
79. Ren, G.; Xu, M.; Chu, Z.; Guo, J.; Li, Q.; Liu, X.; Wang, Y., Changes of surface air temperature in China during 1951–2004. *Climatic and Environmental Research* **2005**, *10* (4), 717-727. 815
80. Trenberth, K. E., Atmospheric moisture residence times and cycling: Implications for rainfall rates and climate change. *Climatic change* **1998**, *39* (4), 667-694. 816
81. Melki, A.; Abida, H., Inter-annual variability of rainfall under an arid climate: case of the Gafsa region, South west of Tunisia. *Arabian Journal of Geosciences* **2018**, *11* (18), 1-13. 817
82. Tu, K.; Yan, Z.; Dong, W., Climatic jumps in precipitation and extremes in drying North China during 1954-2006. *Journal of the Meteorological Society of Japan. Ser. II* **2010**, *88* (1), 29-42. 818
83. You, Q.; Kang, S.; Aguilar, E.; Pepin, N.; Flügel, W.-A.; Yan, Y.; Xu, Y.; Zhang, Y.; Huang, J., Changes in daily climate extremes in China and their connection to the large scale atmospheric circulation during 1961–2003. *Climate Dynamics* **2011**, *36* (11), 2399-2417. 819
84. Charles, R. G.; Davies, M. L.; Douglas, P.; Hallin, I. L., Sustainable solar energy collection and storage for rural Sub-Saharan Africa. In *A comprehensive guide to solar energy systems*, Elsevier: 2018; pp 81-107. 820
85. Rowhani, P.; Lobell, D. B.; Linderman, M.; Ramankutty, N., Climate variability and crop production in Tanzania. *Agricultural and forest meteorology* **2011**, *151* (4), 449-460. 821
86. Pendergrass, A. G.; Knutti, R.; Lehner, F.; Deser, C.; Sanderson, B. M., Precipitation variability increases in a warmer climate. *Scientific reports* **2017**, *7* (1), 1-9. 822
- 823
- 824
- 825
- 826
- 827
- 828
- 829
- 830
- 831
- 832
- 833
- 834
- 835
- 836
- 837
- 838
- 839
- 840
- 841
- 842
- 843
- 844

-
87. Shively, G. E., Infrastructure mitigates the sensitivity of child growth to local agriculture and rainfall in Nepal and Uganda. *Proceedings of the National Academy of Sciences* **2017**, *114* (5), 903-908. 845
846
88. Field, C. B.; Barros, V.; Stocker, T. F.; Dahe, Q., *Managing the risks of extreme events and disasters to advance climate change adaptation: special report of the intergovernmental panel on climate change*. Cambridge University Press: 2012. 847
848
849